

# Associated production of a light Higgs boson and a chargino pair in the MSSM at linear colliders

Giancarlo Ferrera<sup>1,2</sup> and Barbara Mele<sup>2,1</sup>

<sup>1</sup>*Dip. di Fisica, Università La Sapienza, P.le A. Moro 2, I-00185 Rome, Italy*

<sup>2</sup>*Istituto Nazionale di Fisica Nucleare, Sezione di Roma, Rome, Italy*

*E-mail addresses :* *giancarlo.ferrera@roma1.infn.it, barbara.mele@roma1.infn.it*

---

## Abstract

In the Minimal Supersymmetric Standard Model (MSSM), we study the light Higgs-boson radiation off a light-chargino pair in the process  $e^+e^- \rightarrow h \tilde{\chi}_1^+ \tilde{\chi}_1^-$  at linear colliders with  $\sqrt{s} = 500$  GeV. We analyze cross sections in the regions of the MSSM parameter space where the process  $e^+e^- \rightarrow h \tilde{\chi}_1^+ \tilde{\chi}_1^-$  can not proceed via on-shell production and subsequent decay of either heavier charginos or the pseudoscalar Higgs boson  $A$ . In particular, we compute the total cross section and the analytical form of the Higgs-boson momentum distribution, in the limit of heavy electron-sneutrino mass,  $m_{\tilde{\nu}_e} \gg M_W$ . Cross sections up to about 1 fb are allowed, according to present experimental limits on the Higgs-boson and chargino masses. A measurement of the  $e^+e^- \rightarrow h \tilde{\chi}_1^+ \tilde{\chi}_1^-$  production rate would provide a determination of the  $h \tilde{\chi}_1^+ \tilde{\chi}_1^-$  coupling, that is not accessible via Higgs-boson decay channels due to phase-space restrictions.

---

## 1 Introduction

Linear colliders would be a fantastic *precision instrument* for Higgs boson physics and physics beyond the standard model (SM) that could show up at the LHC. In particular, if supersymmetry (SUSY) exists with partners of known particles with masses not too far from present experimental limits, next-generation linear colliders such as TESLA and NLC/JLC [1] would be able to measure (sometimes with excellent precision) a number of crucial parameters (such as masses, couplings and mixing angles),

and eventually test the fine structure of a particular SUSY model. For instance, a linear collider at  $\sqrt{s} = 350\text{-}500$  GeV will be able to disentangle the characteristic two-doublet nature of a light Higgs boson [2] of the Minimal Supersymmetric Standard Model (MSSM) [3, 4, 5] even in the *decoupling* limit, where the light Higgs mimics the SM Higgs behavior, and all the other Higgs bosons and SUSY partners are out of reach of both the LHC and linear colliders.

Quite a few studies have been carried out to establish the linear-collider potential in determining Higgs boson couplings to fermions, vector bosons, and also to SUSY partners [1]. For coupling *suppressed* by the relatively light mass of the coupled particle (as for the light fermions couplings to the Higgs bosons, where  $g_{hff} \sim m_f/v$ ), the coupling is generally determined through the corresponding Higgs decay branching ratio measurement.

On the other hand, since the main Higgs production mechanisms occur through the *unsuppressed* Higgs boson couplings to vector bosons, the analysis of the Higgs boson production cross sections is expected to provide a good determination of the Higgs-bosons couplings to the  $Z$  and  $W$  vector bosons.

Then, there are a number of couplings of the Higgs bosons to quite heavy particles, other than gauge bosons, that can not be investigated through Higgs boson decay channels due to phase-space restrictions. In the latter case, the associated production of a Higgs boson and a pair of the heavy particles, when allowed by phase space, can provide an alternative to measure the corresponding coupling. Some reduction in the rate due to the possible phase-space saturation by the heaviness of the final states is expected in this case.

For instance, the SM Higgs-boson *unsuppressed* coupling to the top quark,  $m_t/v$ , can be determined at linear colliders with  $\sqrt{s} \sim 1$  TeV through the production rates for the Higgs radiated off a top-quark pair in the channel  $e^+e^- \rightarrow h t\bar{t}$  [6].

The latter strategy can be useful also in the MSSM, that introduces an entire spectrum of relatively heavy partners, that in many cases are coupled to Higgs bosons via an *unsuppressed* coupling constant.

A typical example is that of the light Higgs-boson coupling to the light top squark  $h \tilde{t}_1 \tilde{t}_1$ , that can be naturally large. The continuum production  $e^+e^- \rightarrow h \tilde{t}_1 \tilde{t}_1$  has been studied in [7] as a means of determining this coupling (the corresponding channel at hadron colliders has been investigated also in [8]).

Following a similar strategy, in the present work we want to investigate the possibility to measure the light Higgs coupling to light charginos  $h \tilde{\chi}_1^+ \tilde{\chi}_1^-$  through the Higgs boson production in association with a chargino pair at linear colliders

$$e^+e^- \rightarrow h \tilde{\chi}_1^+ \tilde{\chi}_1^- . \quad (1)$$

Note that *heavy* Higgs bosons couplings to SUSY partners can be mostly explored via Higgs decay rates. For instance, heavy Higgs decays into chargino/neutralino pairs and sfermion pairs in the MSSM have been reviewed in [9]. The *precision* measurement of the Higgs-chargino couplings at a muon collider operating at a heavy Higgs boson resonance has been discussed in [10]. On the other hand, as far as the *light* Higgs boson coupling to light charginos is concerned, not much can be learned through Higgs decay channels due to phase-space restrictions. Indeed, in the MSSM  $m_h$  is expected to be lighter than about 130 GeV [11], and the present experimental limit on the chargino mass  $m_{\tilde{\chi}_1^+} > 103.5$  GeV (or even the milder one  $m_{\tilde{\chi}_1^+} > 92.4$  GeV, in case of almost degenerate chargino and lightest neutralino) [12] excludes the decay  $h \rightarrow \tilde{\chi}_1^+ \tilde{\chi}_1^-$ .

Hence, the simplest way to determine the  $h \tilde{\chi}_1^+ \tilde{\chi}_1^-$  coupling could be through the measurement of the rate for the light Higgs-boson production at linear colliders in the channel  $e^+ e^- \rightarrow h \tilde{\chi}_1^+ \tilde{\chi}_1^-$ . The present mass limits allow a good potential for covering a considerable area of the MSSM parameter space, even at  $\sqrt{s} \simeq 500$  GeV.

We will concentrate on the *non resonant* continuum production  $e^+ e^- \rightarrow h \tilde{\chi}_1^+ \tilde{\chi}_1^-$ , that is, we will not include in our study the cases where the considered process proceeds through the on-shell production of either a  $\tilde{\chi}_1^+ \tilde{\chi}_2^-$  (or the charged conjugated  $\tilde{\chi}_1^- \tilde{\chi}_2^+$ ) or a  $hA$  intermediate state (where  $\tilde{\chi}_2^-$  is the heavier chargino and  $A$  is the pseudoscalar Higgs boson) with a subsequent decay  $\tilde{\chi}_2^- \rightarrow h \tilde{\chi}_1^-$  and  $A \rightarrow \tilde{\chi}_1^+ \tilde{\chi}_1^-$ , respectively. In the latter cases, the total  $h \tilde{\chi}_1^+ \tilde{\chi}_1^-$  production rates are in general enhanced with respect to the continuum production, that can be viewed as a higher-order process in the electroweak coupling. We will also assume a large value for the electron sneutrino mass (i.e.,  $m_{\tilde{\nu}_e} > 1$  TeV). This suppresses the Feynman diagrams with a sneutrino exchange, involving predominantly the gaugino components of the charginos.

Note that the SM process  $e^+ e^- \rightarrow HW^+W^-$  (that can be connected by a SuSy transformation to  $e^+ e^- \rightarrow h \tilde{\chi}_1^+ \tilde{\chi}_1^-$ ) has a total cross section of about 5.6 fb for  $m_H \simeq 120$  GeV, at  $\sqrt{s} \simeq 500$  GeV [13].

The measurement of the  $h \tilde{\chi}_1^+ \tilde{\chi}_1^-$  coupling through the process  $e^+ e^- \rightarrow h \tilde{\chi}_1^+ \tilde{\chi}_1^-$  would complement the nice set of precision measurements in the chargino sector expected at future high energy colliders (see [14] and reference therein).

The plan of the paper is the following. In Section 2, the MSSM parameter regions that are of relevance for the non resonant  $h \tilde{\chi}_1^+ \tilde{\chi}_1^-$  production are discussed. We also define three *reference scenarios* for the following analysis. In Section 3, the matrix element for  $e^+ e^- \rightarrow h \tilde{\chi}_1^+ \tilde{\chi}_1^-$  is presented, and the cross-section computation is described. In Section 4, we present total cross sections versus the MSSM parameters.

We also discuss the validity of the assumption of neglecting sneutrino-exchange diagrams. In Section 5, we present Higgs-boson momentum distributions, before giving our conclusions in Section 6. In Appendix A, we define the relevant interaction Lagrangian and couplings. In Appendix B, we describe the phase-space integration that allowed to obtain an analytical form for the Higgs momentum distribution.

## 2 Relevant MSSM Parameter Space

Charginos are expected to be in general among the lightest SuSy partners in the new particle spectrum of the MSSM. This makes interesting to consider the production of a light Higgs boson associated to two light charginos in the process  $e^+e^- \rightarrow h \tilde{\chi}_1^+ \tilde{\chi}_1^-$  at  $\sqrt{s} = 500$  GeV, even if all the particles in the final states are expected to be not so light, and in general heavier than 100 GeV.

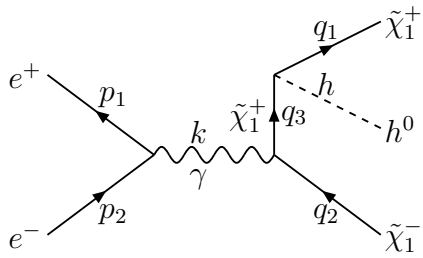
Charginos are the mass eigenstates of the mass matrix that mixes charged gaugino and higgsino states (see [4], and Appendix A). At tree level, the latter depends on three parameters,  $M_2$ ,  $\mu$  and  $\tan\beta$ . When the mass matrix is real, the two diagonalizing matrices can be expressed in terms of two mixing angles,  $\phi_{\pm}$ . Then, the mass eigenvalues  $m_{\tilde{\chi}_1^+}$  and  $m_{\tilde{\chi}_2^+}$  and the mixing angles can be analytically written in terms of the parameters  $M_2$ ,  $\mu$  and  $\tan\beta$ . The presence of a Higgs boson in the process  $e^+e^- \rightarrow h \tilde{\chi}_1^+ \tilde{\chi}_1^-$  requires at tree level a further parameter, that can be the pseudoscalar mass  $m_{A^0}$ . On the other hand, the inclusion of the main radiative corrections to the Higgs boson mass and couplings involves all the basic parameters needed for setting the complete mass spectrum of the SuSy partners in the MSSM. In our study of  $e^+e^- \rightarrow h \tilde{\chi}_1^+ \tilde{\chi}_1^-$  at  $\sqrt{s} = 500$  GeV, we set  $m_{A^0} = 500$  GeV. This pushes the pseudoscalar field  $A^0$  beyond the threshold for direct production, thus preventing resonant  $A^0 \rightarrow \tilde{\chi}_1^+ \tilde{\chi}_1^-$  contribution to the  $h \tilde{\chi}_1^+ \tilde{\chi}_1^-$  final state. At the same time, such a large value for  $m_{A^0}$  sets a *decoupling-limit* scenario ( $m_{A^0} \gg M_Z$ ).

Present experimental lower limits on  $m_h$  [15] in the *decoupling-limit* MSSM are close to the ones derived from the SM Higgs boson direct search (i.e.,  $m_H > 114.4$  GeV at 95% C.L. [16]).

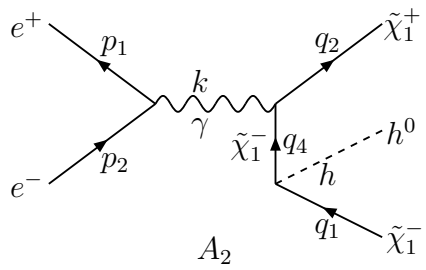
The corrections to the light Higgs mass and coupling parameter  $\alpha^*$  (cf. Appendix A) have been computed according to the code FeynHiggsFast [17], with the following input parameters :  $M_{\tilde{t}_{L,R}} = M_{\tilde{b}_{L,R}} = M_{\tilde{g}} = 1$  TeV ,  $X_t$  ( $\equiv A_t - \mu \cot\beta$ ) =

---

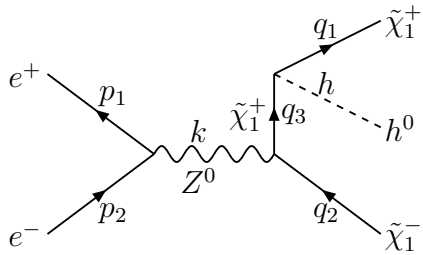
\*The inclusion of radiative corrections to the Higgs-boson coupling would require in principle a more general treatment of the complete set of radiative corrections to the process under consideration. On the other hand, one can see that the simple inclusion of the correction to the parameter  $\alpha$  is to a good extent self consistent in our case. The latter has anyway a minor impact on our results.



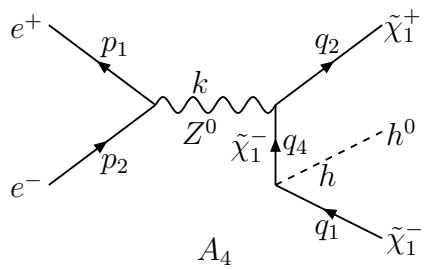
$A_1$



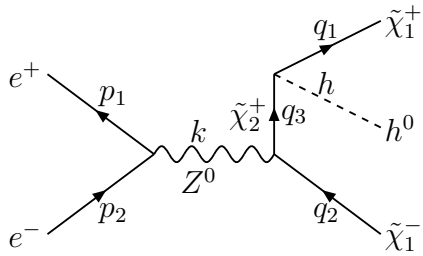
$A_2$



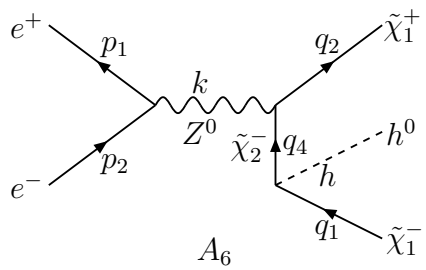
$A_3$



$A_4$



$A_5$



$A_6$

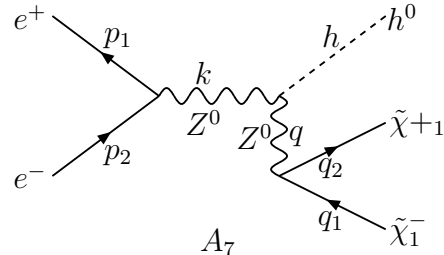


Figure 1: Set of Feynman diagrams included in the analytic Higgs-boson distribution.

either 0 or 2 TeV,  $A_b = A_t$ ,  $m_t = 175$  GeV,  $m_b = 4.5$  GeV,  $\mu = 200$  GeV,  $M_2 = 400$  GeV, and renormalization scale at  $m_t$ , in the most complete version of the code <sup>†</sup>.

<sup>†</sup>Varying the  $\mu$  and  $M_2$  parameters would affect the Higgs spectrum and couplings negligibly.

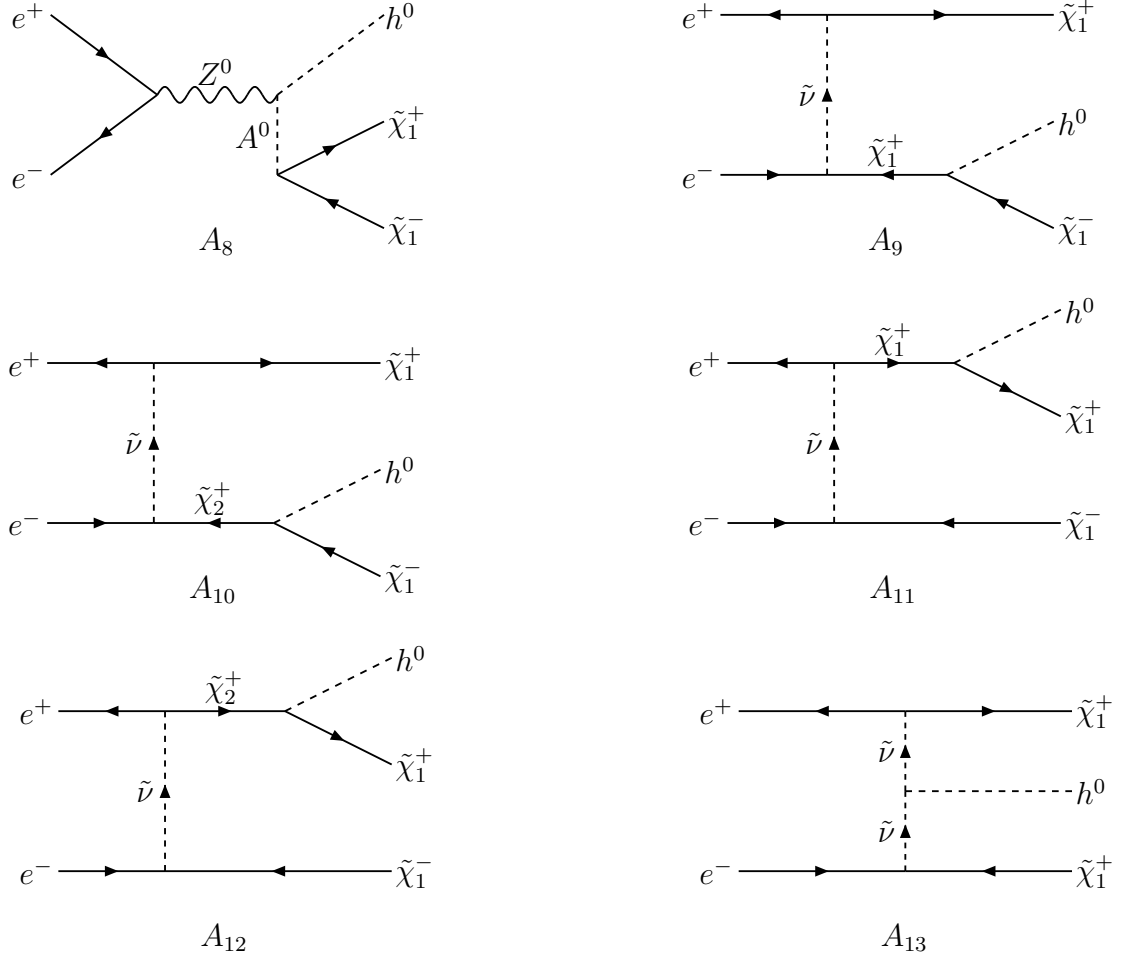


Figure 2: Set of Feynman diagrams not included in the analytic Higgs-boson distribution.

Then, in our study, we assumed three different  $\tan \beta$  scenarios, and corresponding  $m_h$  values for  $m_{A^0} = 500$  GeV:

- a)**  $\tan \beta = 3$ , with *maximal* stop mixing (i.e.,  $X_t = 2$  TeV), and  $m_h = 120.8$  GeV;
- b)**  $\tan \beta = 15$ , with *no* stop mixing (i.e.,  $X_t = 0$ ), and  $m_h = 114.3$  GeV;
- c)**  $\tan \beta = 30$ , with *maximal* stop mixing (i.e.,  $X_t = 2$  TeV), and  $m_h = 132.0$  GeV;

that are allowed by present experimental limits [15].

The 13 Feynman diagrams corresponding to the process  $e^+e^- \rightarrow h \tilde{\chi}_1^+ \tilde{\chi}_1^-$  arise either from the *s*-channel  $Z^0/\gamma$  exchange or from the *t*-channel electron-sneutrino  $\tilde{\nu}_e$

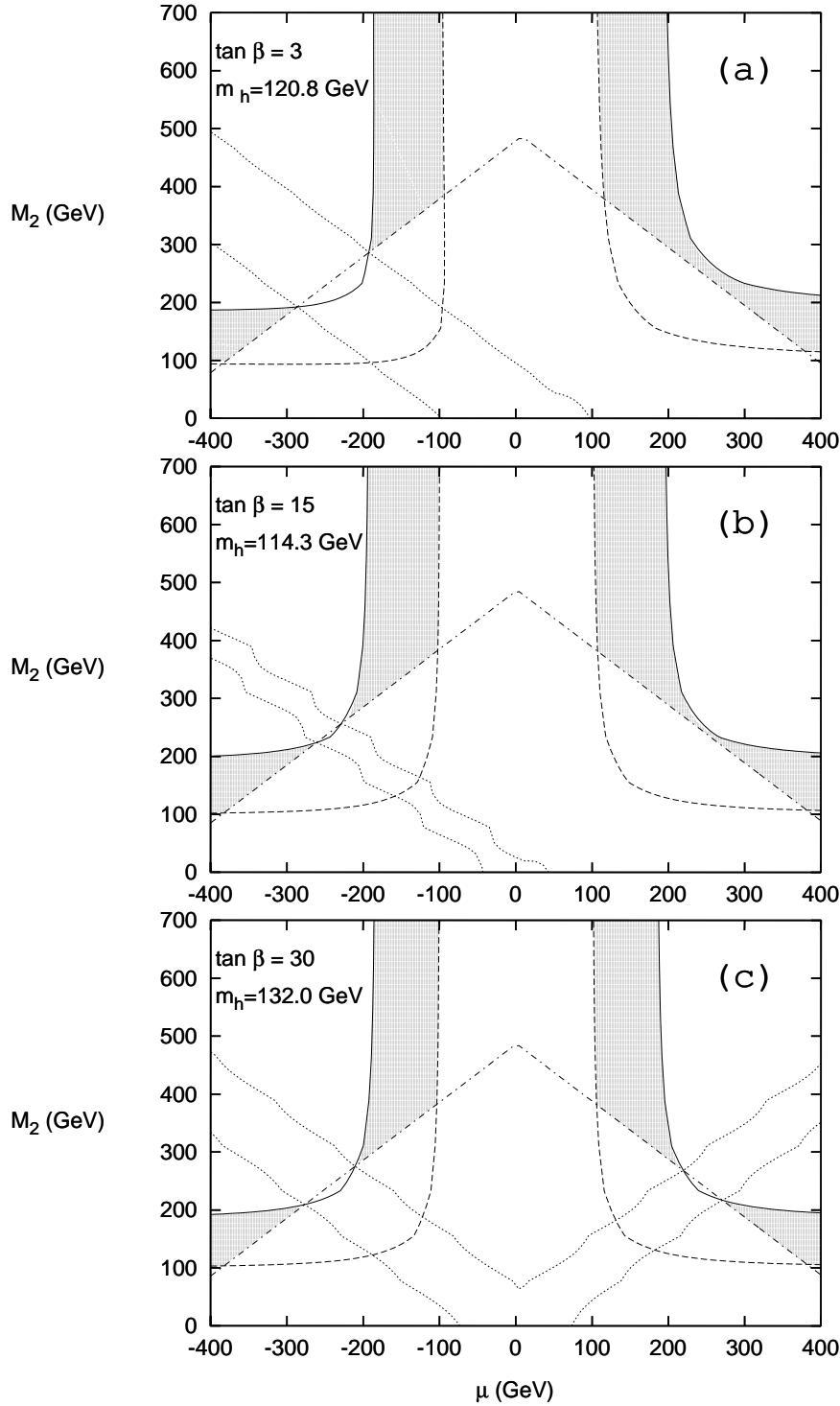


Figure 3: Parameter regions allowed for the continuum production  $e^+e^- \rightarrow h \tilde{\chi}_1^+\tilde{\chi}_1^-$  at  $\sqrt{s} = 500$  GeV, for  $\tan \beta = 3, 15, 30$  and  $M_{A^0} = 500$  GeV (in grey).

exchange. In our cross-section evaluation, we include only the 7 *s*-channel  $Z^0/\gamma$  exchange diagrams reported in Fig. 1, and disregard the 6 diagrams in Fig. 2. The latter are expected to contribute moderately to the cross section in the case  $m_{\tilde{\nu}_e} > 1$  TeV,  $m_{A^0} = 500$  GeV. We will discuss the accuracy of this assumption in Section 4.

In Fig. 3, we show (in grey), for the three different  $\tan \beta$  scenarios, the area in the  $(\mu, M_2)$  plane that is of relevance for the *non resonant*  $e^+e^- \rightarrow h \tilde{\chi}_1^+\tilde{\chi}_1^-$  process. The solid lines correspond to the threshold energy contour level :

$$\sqrt{s} = 2 m_{\tilde{\chi}_1^+} + m_h, \quad (2)$$

while the dashed lines refer to the experimental limit on the light chargino mass ( $m_{\tilde{\chi}_1^+} \simeq 100$  GeV).

The straight dot-dashed lines limit from above the region that allows the associated production of a light chargino  $\tilde{\chi}_1^+$  and a resonant heavier chargino  $\tilde{\chi}_2^-$  (that we are not interested in), and correspond to :

$$\sqrt{s} = m_{\tilde{\chi}_1^+} + m_{\tilde{\chi}_2^-}. \quad (3)$$

A further region of interest (beyond the grey one) could be the one where, although  $\sqrt{s} > m_{\tilde{\chi}_1^+} + m_{\tilde{\chi}_2^-}$ , the heavier chargino is *below* the threshold for a direct decay  $\tilde{\chi}_2^+ \rightarrow \tilde{\chi}_1^+ h$ . Then, again a resonant  $\tilde{\chi}_2^+$  would not be allowed. The area where  $m_{\tilde{\chi}_2^+} < m_{\tilde{\chi}_1^+} + m_h$  is the one inside the oblique stripes in Fig. 3. The intersection of these stripes with the area between the solid and dashed curves is a further (although quite restricted) region relevant to the non resonant  $e^+e^- \rightarrow h \tilde{\chi}_1^+\tilde{\chi}_1^-$  process. In our analysis, we did not include this parameter region, since this would have required some further dedicated elaboration of the analytic form for the  $e^+e^- \rightarrow h \tilde{\chi}_1^+\tilde{\chi}_1^-$  distributions.

### 3 Cross Section Evaluation

In this section, we describe how we worked out an analytic form for the Higgs momentum distribution in the process  $e^+e^- \rightarrow h \tilde{\chi}_1^+\tilde{\chi}_1^-$ . As anticipated in Section 2, our analysis concentrates on the set of 7 Feynman diagrams presented in Fig. 1. Our evaluation will then be particularly suitable in case of heavy electron sneutrinos. We will discuss quantitatively this point in Section 4.

The matrix elements corresponding to the amplitudes  $A_1, \dots, A_7$  in Fig. 1 are :

$$\mathcal{M}_1 = \frac{ig e^2}{k^2 + i\epsilon} \bar{u}_{s_1}^\chi(q_1) \left( C_{11}^L P_L + C_{11}^R P_R \right) \frac{(\not{q}_3 + M_1)}{q_3^2 - M_1^2 + i\epsilon} \gamma^\mu v_{s_2}^\chi(q_2) \bar{v}_{r_1}^e(p_1) \gamma_\mu u_{r_2}^e(p_2)$$

$$\begin{aligned}
\mathcal{M}_2 &= \frac{ig^2}{k^2 + i\epsilon} \bar{u}_{s_1}^\chi(q_1) \gamma^\mu \frac{(-\not{q}_4 + M_1)}{q_4^2 - M_1^2 + i\epsilon} \left( C_{11}^L P_L + C_{11}^R P_R \right) v_{s_2}^\chi(q_2) \bar{v}_{r_1}^e(p_1) \gamma_\mu u_{r_2}^e(p_2) \\
\mathcal{M}_3 &= \frac{-ig^3}{4 \cos^2 \theta_w (k^2 - M_Z^2 + i\epsilon)} \bar{u}_{s_1}^\chi(q_1) \left( C_{11}^L P_L + C_{11}^R P_R \right) \frac{(\not{q}_3 + M_1)}{q_3^2 - M_1^2 + i\epsilon} \gamma^\mu \\
&\quad \times \left( O_{11}^L P_L + O_{11}^R P_R \right) v_{s_2}^\chi(q_2) \left( g_{\mu\nu} - \frac{k_\mu k_\nu}{M_Z^2} \right) \bar{v}_{r_1}^e(p_1) \gamma^\nu (g_V - \gamma_5) u_{r_2}^e(p_2) \\
\mathcal{M}_4 &= \frac{-ig^3}{4 \cos^2 \theta_w (k^2 - M_Z^2 + i\epsilon)} \bar{u}_{s_1}^\chi(q_1) \gamma^\mu \left( O_{11}^L P_L + O_{11}^R P_R \right) \frac{(-\not{q}_4 + M_1)}{q_4^2 - M_1^2 + i\epsilon} \\
&\quad \times \left( C_{11}^L P_L + C_{11}^R P_R \right) v_{s_2}^\chi(q_2) \left( g_{\mu\nu} - \frac{k_\mu k_\nu}{M_Z^2} \right) \bar{v}_{r_1}^e(p_1) \gamma^\nu (g_V - \gamma_5) u_{r_2}^e(p_2) \\
\mathcal{M}_5 &= \frac{-ig^3}{4 \cos^2 \theta_w (k^2 - M_Z^2 + i\epsilon)} \bar{u}_{s_1}^\chi(q_1) \left( C_{12}^L P_L + C_{12}^R P_R \right) \frac{(\not{q}_3 + M_2)}{q_3^2 - M_2^2 + i\epsilon} \gamma^\mu \\
&\quad \times \left( O_{21}^L P_L + O_{21}^R P_R \right) v_{s_2}^\chi(q_2) \left( g_{\mu\nu} - \frac{k_\mu k_\nu}{M_Z^2} \right) \bar{v}_{r_1}^e(p_1) \gamma^\nu (g_V - \gamma_5) u_{r_2}^e(p_2) \\
\mathcal{M}_6 &= \frac{-ig^3}{4 \cos^2 \theta_w (k^2 - M_Z^2 + i\epsilon)} \bar{u}_{s_1}^\chi(q_1) \gamma^\mu \left( O_{12}^L P_L + O_{12}^R P_R \right) \frac{(-\not{q}_4 + M_2)}{q_4^2 - M_2^2 + i\epsilon} \\
&\quad \times \left( C_{21}^L P_L + C_{21}^R P_R \right) v_{s_2}^\chi(q_2) \left( g_{\mu\nu} - \frac{k_\mu k_\nu}{M_Z^2} \right) \bar{v}_{r_1}^e(p_1) \gamma^\nu (g_V - \gamma_5) u_{r_2}^e(p_2) \\
\mathcal{M}_7 &= \frac{ig^3 M_Z \sin(\beta - \alpha)}{4 \cos^3 \theta_w} \bar{u}_{s_1}^\chi(q_1) \gamma^\mu \left( O_{11}^L P_L + O_{11}^R P_R \right) v_{s_2}^\chi(q_2) \\
&\quad \times \frac{(g_{\mu\nu} - q_\mu q_\nu / M_Z^2)}{(q^2 - M_Z^2 + i\epsilon)} \frac{(g^{\nu\sigma} - k^\nu k^\sigma / M_Z^2)}{(k^2 - M_Z^2 + i\epsilon)} \bar{v}_{r_1}^e(p_1) \gamma_\sigma (g_V - \gamma_5) u_{r_2}^e(p_2), \tag{4}
\end{aligned}$$

where

$$k = p_1 + p_2 = q_1 + q_2 + h, \quad q_3 = q_1 + h, \quad q_4 = q_2 + h, \quad q = p_1 + p_2 - h,$$

and  $M_{1,2} = m_{\tilde{\chi}_{1,2}^\pm}$ .

All external momenta are defined in Fig. 1, as flowing from the left to the right, and different couplings in Eq. (4) are defined in Appendix A. The lower indices of the spinors  $u, v$  refer to the particle spin.

We squared, averaged over the initial spin, and summed over the final spin the sum of the matrix elements in Eq. (4) with the help of FORM [18]. Then, we performed a double analytic integration over the phase-space variables according to the procedure described in Appendix B. This allowed us to obtain an exact *analytic* expression for the Higgs-boson momentum distribution

$$E_h \frac{d\sigma}{d^3 \mathbf{h}} = \frac{\beta}{s(4\pi)^5} \int_{-1}^1 d\cos\vartheta \int_0^{2\pi} d\varphi |\mathcal{M}|^2 = f(p_1, p_2, h). \tag{5}$$

The notation is according to Appendix B, and  $\mathcal{M} = \sum_{i=1}^7 \mathcal{M}_i$ . The complete code, including the analytic result for  $E_h \frac{d\sigma}{d^3 \mathbf{h}}$  (that is a quite lengthy expression), and the

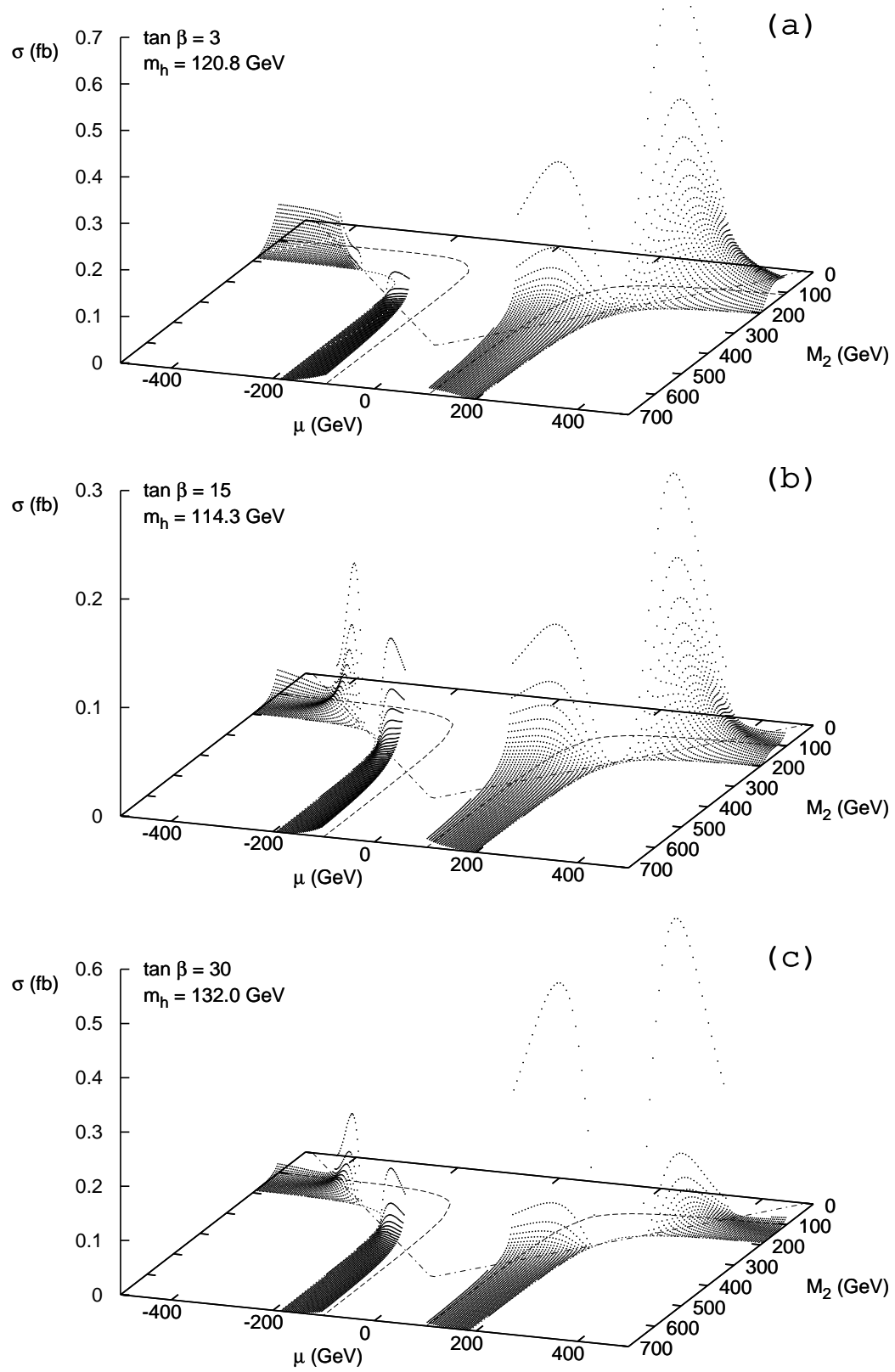


Figure 4: Total cross section for  $e^+e^- \rightarrow h \tilde{\chi}_1^+ \tilde{\chi}_1^-$  at  $\sqrt{s} = 500$  GeV, for  $\tan \beta = 3, 15, 30$  and  $M_{A^0} = 500$  GeV.

$\tan \beta$	$\mu$	$M_2$	$\sigma (fb)$	$\Delta (\%)$ $m_{\tilde{\nu}} = 200 \text{ GeV}$	$\Delta (\%)$ $m_{\tilde{\nu}} = 1 \text{ TeV}$	$\Delta (\%)$ $m_{\tilde{\nu}} = 3 \text{ TeV}$	$m_h$	$\cos \alpha$
3	400	150	$1.3 \times 10^{-1}$	96	43	4.1	120.0	0.939
	-400	150	$1.2 \times 10^{-2}$	267	19	1.9	119.1	0.940
	150	700	$9.1 \times 10^{-3}$	-57	-7.2	-0.76	120.9	0.939
	-150	700	$4.6 \times 10^{-3}$	37	12	1.3	120.4	0.939
15	400	150	$3.2 \times 10^{-2}$	212	43	4.1	113.7	0.997
	-400	150	$4.9 \times 10^{-3}$	151	44	4.4	113.8	0.997
	150	700	$2.6 \times 10^{-3}$	-69	-4.0	-0.30	112.7	0.997
	-150	700	$1.6 \times 10^{-3}$	-36	18	2.1	112.8	0.997
30	400	150	$1.6 \times 10^{-2}$	178	46	4.4	126.2	0.999
	-400	150	$6.1 \times 10^{-1}$	171	49	4.7	127.5	0.999
	150	700	$1.3 \times 10^{-3}$	-66	1.8	0.43	131.5	0.999
	-150	700	$1.1 \times 10^{-3}$	-52	13	1.6	130.6	0.999

Table 1: Comparison of the cross section  $\sigma$  corresponding to the diagrams in Fig. 1, with the one including also the diagrams in Fig. 2, computed by CompHEP. The quantities  $(\mu, M_2, m_h)$  are in GeV, and  $\Delta$  is defined as in Eq. (6).

numerical integration routine that allows a fast evaluation of the total cross section, is available from the authors' e-mail addresses.

## 4 Total Cross Sections

In Figs. 4–6, we show the total cross sections for  $e^+e^- \rightarrow h \tilde{\chi}_1^+ \tilde{\chi}_1^-$  at  $\sqrt{s} = 500 \text{ GeV}$ . We obtained them by numerically integrating over the Higgs-boson energy and angle the analytic distribution in Eq. (5) (see Appendix B), in the three scenarios **a**, **b**, **c** defined in Section 2. In Fig. 4, we scan the relevant  $(\mu, M_2)$  parameter space for  $|\mu| < 500 \text{ GeV}$ , and  $M_2 < 700 \text{ GeV}$ . Cross sections of a few  $0.1 \text{ fb}^{-1}$  are reached in a good portion of the allowed regions, especially in the maximal-mixing scenarios **a** and **c**, and for positive  $\mu$ . More accurate information can be obtained from the two-dimensional plots in Figs. 5 and 6 (at fixed  $M_2$  and  $\mu$  values, respectively). We checked that our results completely agree with the cross section evaluated by CompHEP [19] on the basis of the same set of Feynman diagrams of Fig. 1.

We studied quantitatively the consequence of disregarding the 6 diagrams in Fig. 2, involving either pseudoscalar or sneutrino exchange, by comparing our results with the cross section corresponding to the complete set of 13 diagrams, computed by CompHEP. While the pseudoscalar-exchange diagram never contributes sizable for  $m_{A^0} = 500 \text{ GeV}$ , the influence of the 5 sneutrino-exchange diagrams depends critically

on  $m_{\tilde{\nu}_e}$ , and, to a good extend, also on the relative importance of the gaugino-higgsino components in the chargino. In Table 1, for different MSSM parameter values, we present first the cross section  $\sigma$  computed by integrating Eq. (5), and then the quantity

$$\Delta (\%) = \frac{\sigma - \sigma_{CHEP}}{\sigma_{CHEP}} \times 100 , \quad (6)$$

that is its corresponding percentage difference with the CompHEP evaluation  $\sigma_{CHEP}$  based on the complete set of 13 diagrams, versus  $m_{\tilde{\nu}_e}$ , for  $m_{\tilde{\nu}_e} = 0.2, 1$  and  $3$  TeV. In this comparison, we assumed, for the Higgs mass  $m_h$  and coupling  $\cos \alpha$ , the values used by CompHEP (shown in Table 1), that are estimated in a slightly different approximation from the one adopted in this paper. Regarding the  $(\mu, M_2)$  parameter choice, in Table 1, for each  $\tan \beta$  value, we set two points at  $\mu = \pm 400$  GeV and  $M_2 = 150$  GeV, that are close to *gaugino dominance* in the light charginos, and two points at  $\mu = \pm 150$  GeV and  $M_2 = 700$  GeV, for which instead the *higgsino* component is enhanced. Since, gauginos/higgsinos couple dominantly to the sneutrino/ $Z^0$ , one expects, for the latter set of  $(\mu, M_2)$  values, the total cross section be less sensitive to the inclusion of sneutrino-exchange diagrams. This behavior is confirmed in Table 1, where one can see that, for  $M_2 = 700$  GeV (i.e., higgsino dominance),  $\sigma$  differs from  $\sigma_{CHEP}$  by  $(2 - 18)\%$  in all the cases considered at  $m_{\tilde{\nu}_e} = 1$  TeV. At  $m_{\tilde{\nu}_e} = 3$  TeV, our results approximate the complete computation within a few percent in all the relevant parameter space. On the other hand, at lower sneutrino masses ( $m_{\tilde{\nu}_e} \sim 200$  GeV), our approximation turns out to be always quite poor.

We also considered the  $e^+e^- \rightarrow h \tilde{\chi}_1^+ \tilde{\chi}_1^-$  cross sections at the higher-energy extension expected for a linear-collider project [1]. Going at  $\sqrt{s} \simeq 1$  TeV, our treatment of the  $e^+e^- \rightarrow h \tilde{\chi}_1^+ \tilde{\chi}_1^-$  cross section becomes less accurate. Indeed, on the one hand, the  $1/s, 1/(s - M_Z^2)$  dependence of the amplitudes in the diagrams of Fig. 1 makes our cross section decrease with the c.m. energy of the process, in any point of the MSSM parameter space. On the other hand, the relative weight of the amplitudes for the  $t$ -channel exchange of sneutrinos (that we are not taking into account in our evaluation) is expected to increase with  $\sqrt{s}$ .

Anyway, as far as production rates are concerned, for chargino and Higgs-boson masses not much heavier than present experimental limits, and heavy sneutrinos, the  $\sqrt{s} = 500$  GeV phase of the linear collider could be the best option to study the process  $e^+e^- \rightarrow h \tilde{\chi}_1^+ \tilde{\chi}_1^-$ .

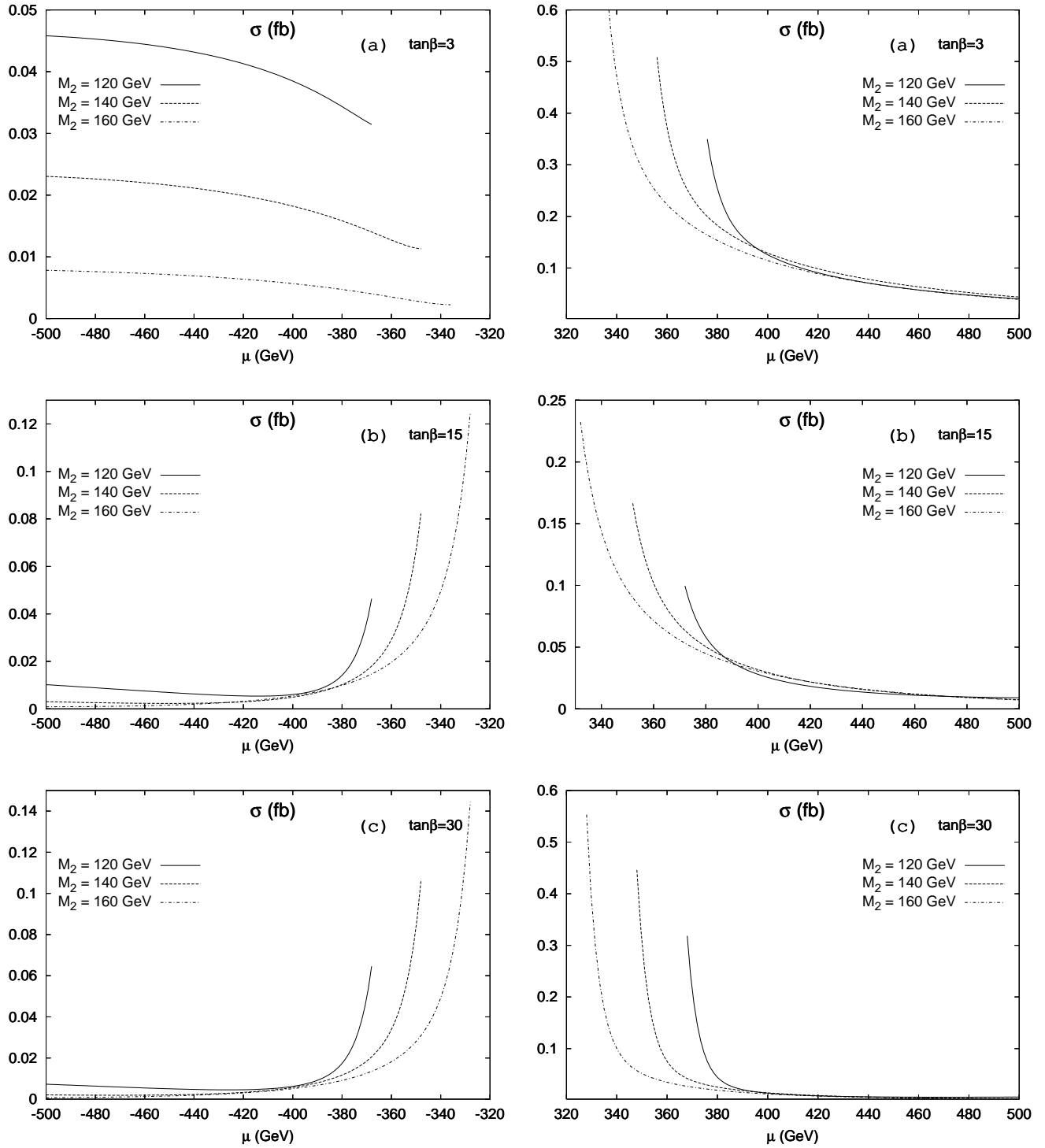


Figure 5: Total cross section for  $e^+e^- \rightarrow h \tilde{\chi}_1^+ \tilde{\chi}_1^-$  at  $\sqrt{s} = 500$  GeV, for  $\tan\beta = 3, 15, 30$ ,  $M_{A^0} = 500$  GeV, and fixed  $M_2$  values, versus  $\mu$ .

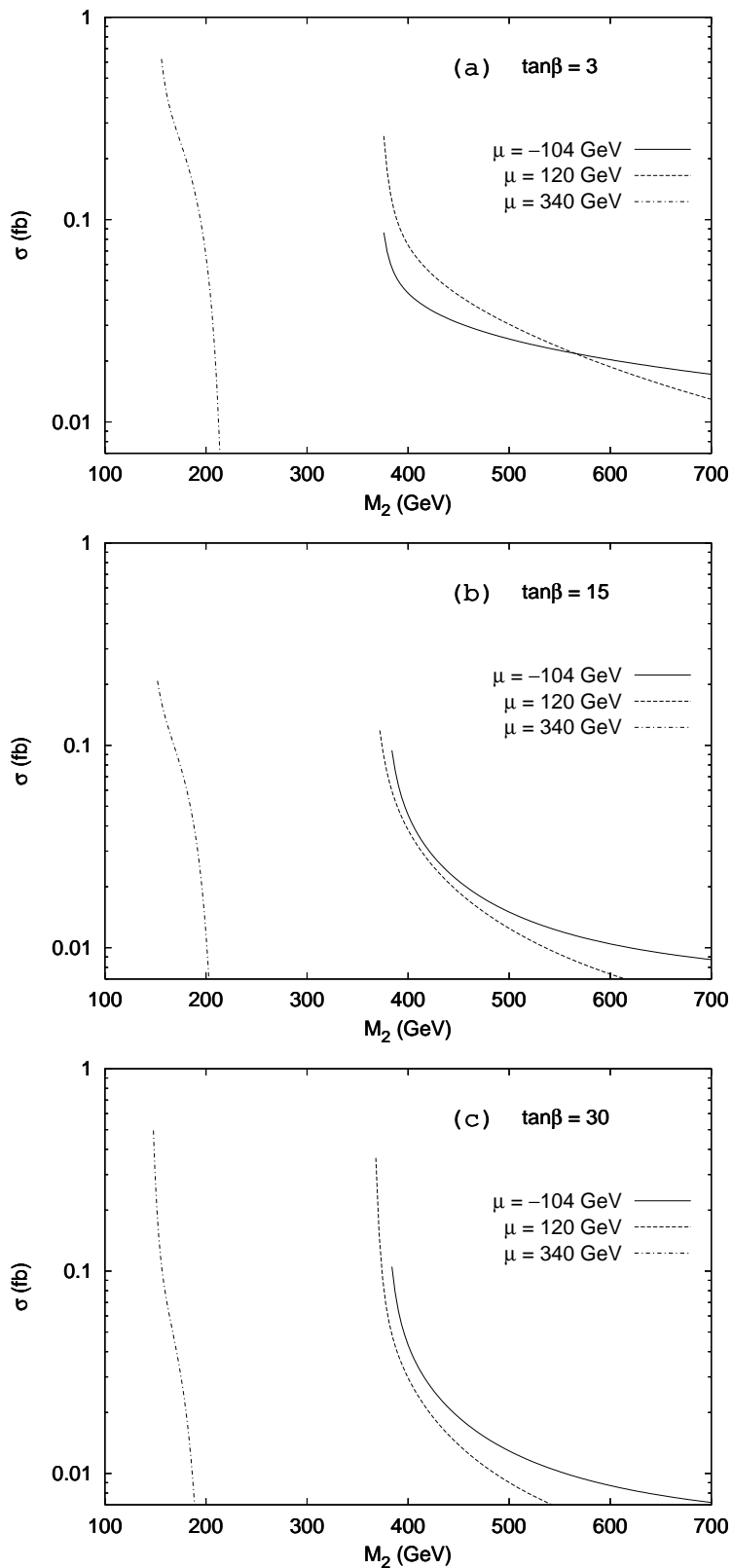


Figure 6: Total cross section for  $e^+e^- \rightarrow h \tilde{\chi}_1^+ \tilde{\chi}_1^-$  at  $\sqrt{s} = 500$  GeV, for  $\tan\beta = 3, 15, 30$ ,  $M_{A^0} = 500$  GeV, and fixed  $\mu$  values, versus  $M_2$ .

## 5 Higgs-boson Momentum Distributions

We finally studied the behavior of Higgs-boson energy and angular distributions versus the MSSM parameters. In Figs. 7 and 8, we plot energy and angular distributions in the  $e^+e^-$  c.m. frame, as obtained by numerically integrating over one variable Eq. (5). We assume the three scenarios **a**, **b**, **c**, defined in Section 2, and  $(\mu, M_2)$  fixed at the following values:  $(350, 150), (150, 350), (120, 600)$  GeV. Both the energy- and angular-distribution shapes are considerably influenced by the gaugino/higgsino composition of the light chargino, and by a possible saturation of the available phase-space.

## 6 Conclusions

In this paper, we analyzed the associated (non resonant) production of a light Higgs boson and a light-chargino pair in the MSSM at linear colliders. In the limit of heavy sneutrino masses ( $m_{\tilde{\nu}_e} > 1$  TeV), we presented total cross sections and distributions in the Higgs-boson momentum. We also worked out an analytical expression for  $E_h \frac{d\sigma}{d^3\mathbf{h}}$  that allows a very fast and accurate determination of the cross section with respect to highly-automated computer codes for cross-section evaluation of generic tree-level processes, that are available in the literature. Cross sections up to a few 0.1 fb (for  $\mu > 0$ ) are obtained for masses not much heavier than present experimental limits. These rates could allow a first determination of the  $h \tilde{\chi}_1^+ \tilde{\chi}_1^-$  coupling, if an integrated luminosity of the order of  $1000 \text{ fb}^{-1}$  will be collected at the  $e^+e^-$  collider with  $\sqrt{s} = 500 \text{ GeV}$ . This would correspond to a statistical error on the production rate of the order of 10%. Since one does not expect important backgrounds from different production channels, one can roughly extrapolate the latter to a determination of the  $h \tilde{\chi}_1^+ \tilde{\chi}_1^-$  coupling with comparable accuracy. Of course, the latter crucially depends on the production rate, that varies largely in the MSSM parameter space covered by the  $h \tilde{\chi}_1^+ \tilde{\chi}_1^-$  production. Further analysis of this measurement, taking into account various systematics, backgrounds, and the fact that a few of the diagrams in Fig. 1 do not depend on the  $h \tilde{\chi}_1^+ \tilde{\chi}_1^-$  coupling will be needed in order to assess on more solid grounds the potential of the process  $e^+e^- \rightarrow h \tilde{\chi}_1^+ \tilde{\chi}_1^-$  for a measurement of the  $h \tilde{\chi}_1^+ \tilde{\chi}_1^-$  coupling.

## Acknowledgments

We thank S. Heinemeyer, A. Pukhov, and P. Slavich for useful discussions.

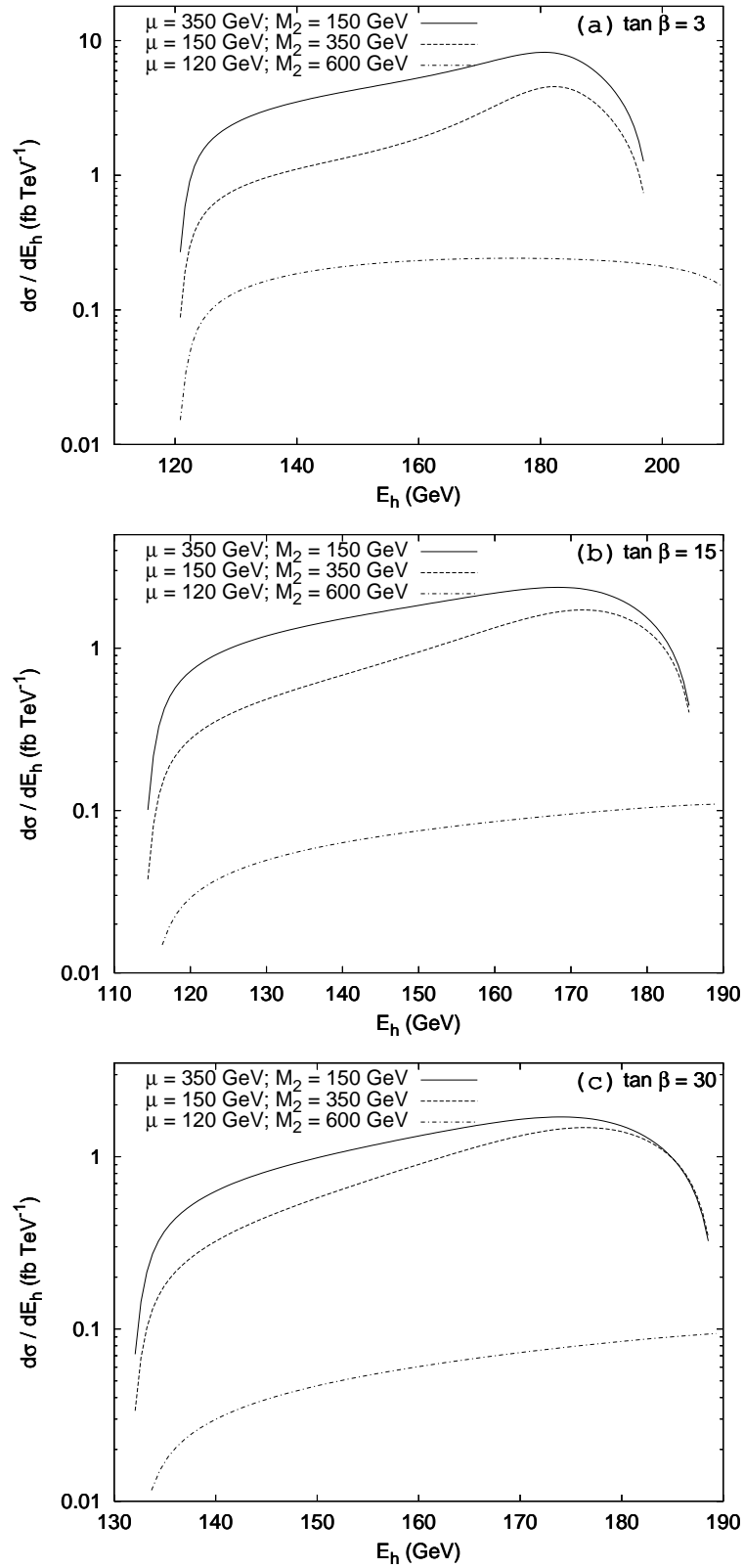


Figure 7: Higgs-boson energy distribution in the  $e^+e^-$  c.m. frame in  $e^+e^- \rightarrow h \tilde{\chi}_1^+\tilde{\chi}_1^-$  at  $\sqrt{s} = 500$  GeV, for  $\tan \beta = 3, 15, 30$ ,  $M_{A^0} = 500$  GeV.

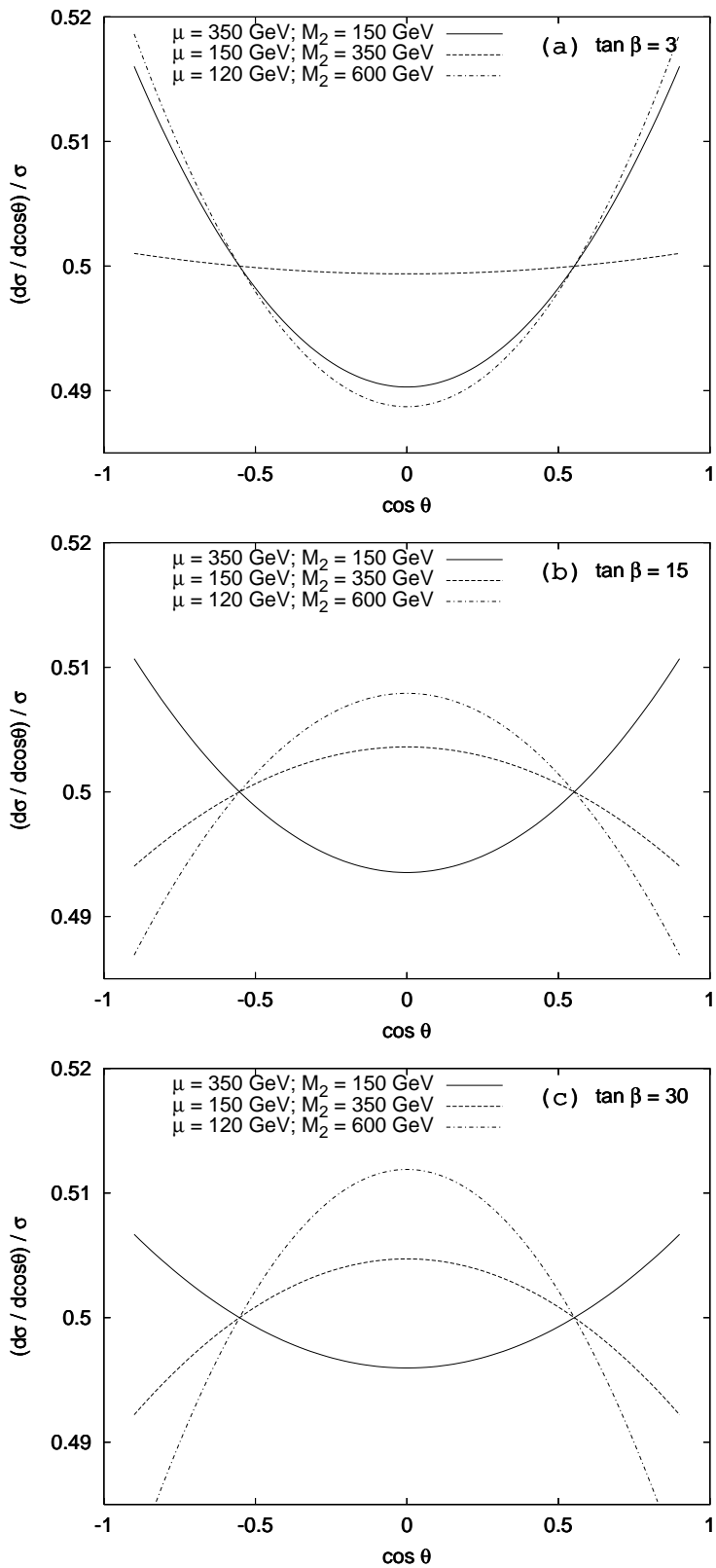


Figure 8: Higgs-boson angular distribution in the  $e^+e^-$  c.m. frame in  $e^+e^- \rightarrow h \tilde{\chi}_1^+\tilde{\chi}_1^-$  at  $\sqrt{s} = 500 \text{ GeV}$ , for  $\tan\beta = 3, 15, 30$ ,  $M_{A^0} = 500 \text{ GeV}$ .

## Appendix A: Feynman Rules

The aim of this Appendix is to define the couplings, parameters, and constants that have been used in this paper, following the conventions in [4]. In the evaluation of the cross section for the process  $e^+e^- \rightarrow h \tilde{\chi}_1^+\tilde{\chi}_1^-$ , we used the Feynman rules corresponding to the following interaction Lagrangian

- $\mathcal{L}_{\gamma e^-e^+} = e A^\mu(x) \bar{e}(x) \gamma_\mu e(x) ,$
- $\mathcal{L}_{Z^0 e^-e^+} = \frac{g}{\cos \theta_w} Z^\mu(x) \bar{e}(x) \gamma_\mu (1 - 4 \sin^2 \theta_w - \gamma_5) e(x) ,$
- $\mathcal{L}_{\gamma \tilde{\chi}_i^+ \tilde{\chi}_j^-} = -e A^\mu(x) \bar{\tilde{\chi}}_i(x) \gamma_\mu \tilde{\chi}_j(x) \delta_{ij} ,$
- $\mathcal{L}_{Z^0 \tilde{\chi}_i^+ \tilde{\chi}_j^-} = \frac{g}{\cos \theta_w} Z^\mu(x) \bar{\tilde{\chi}}_i(x) \gamma_\mu (O'_{ij}^L P_L + O'_{ij}^R P_R) \tilde{\chi}_j(x) ,$
- $\mathcal{L}_{h^0 Z^0 Z^0} = \frac{g m_Z}{\cos \theta_w} Z^\mu(x) Z_\mu(x) h(x) \sin(\beta - \alpha) ,$
- $\mathcal{L}_{h^0 \tilde{\chi}_i^+ \tilde{\chi}_j^-} = g \bar{\tilde{\chi}}_i(x) (C_{ij}^L P_L + C_{ij}^R P_R) \tilde{\chi}_j(x) h(x) ,$

where

$$P_L = \frac{1}{2}(1 - \gamma_5), \quad P_R = \frac{1}{2}(1 + \gamma_5) \quad (7)$$

$$O'_{ij}^L = -V_{i1}V_{j1}^* - \frac{1}{2}V_{i2}V_{j2}^* + \delta_{ij} \sin^2 \theta_w \quad (8)$$

$$O'_{ij}^R = -U_{i1}^*V_{j1} - \frac{1}{2}U_{i2}^*V_{j2} + \delta_{ij} \sin^2 \theta_w \quad (9)$$

and

$$\mathbf{U} = \begin{pmatrix} \cos \phi_- & \sin \phi_- \\ -\sin \phi_- & \cos \phi_- \end{pmatrix} \quad (10)$$

$$\mathbf{V} = \begin{pmatrix} \cos \phi_+ & \sin \phi_+ \\ -\sin \phi_+ & \cos \phi_+ \end{pmatrix} \quad (11)$$

$$\tan(2\phi_-) = 2\sqrt{2}m_W \frac{\mu \sin \beta + M_2 \cos \beta}{M_2^2 - \mu^2 - 2m_W^2 \cos(2\beta)} \quad (12)$$

$$\tan(2\phi_+) = 2\sqrt{2}m_W \frac{\mu \cos \beta + M_2 \sin \beta}{M_2^2 - \mu^2 + 2m_W^2 \cos(2\beta)} . \quad (13)$$

$\mathbf{U}$  and  $\mathbf{V}$  are  $2 \times 2$  unitary matrices that diagonalize the chargino mass matrix  $\mathbf{X}$

$$\mathbf{U}^* \mathbf{X} \mathbf{V}^{-1} = \text{Diag}(m_{\tilde{\chi}_1^\pm}, m_{\tilde{\chi}_2^\pm}) \quad (14)$$

$$\begin{aligned} m_{\tilde{\chi}_1^\pm}^2, m_{\tilde{\chi}_2^\pm}^2 &= \frac{1}{2} \left[ (|M_2|^2 + |\mu|^2 + 2m_W^2) \right. \\ &\quad \left. \mp \sqrt{(|M_2|^2 + |\mu|^2 + 2m_W^2)^2 - 4|\mu M_2 - m_W^2 \sin 2\beta|^2} \right] . \end{aligned} \quad (15)$$

Furthermore,

$$C_{ij}^L = \sin \alpha Q_{ij}^* - \cos \alpha S_{ij}^* \quad (16)$$

$$C_{ij}^R = \sin \alpha Q_{ji} - \cos \alpha S_{ji} \quad (17)$$

$$\text{where } Q_{ij} = \frac{1}{\sqrt{2}} U_{i2} V_{j1}, \quad S_{ij} = \frac{1}{\sqrt{2}} U_{i1} V_{j2},$$

$$\text{and } \tan \beta = \frac{v_2}{v_1}, \quad \tan(2\alpha) = \tan(2\beta) \left( \frac{m_{H^0}^2 + m_{h^0}^2}{m_{A^0}^2 + m_Z^2} \right).$$

## Appendix B : Analytic Integration of the Squared Matrix Element

In this Appendix, we show the procedure we followed in order to get an analytic expression for the Higgs-boson momentum distribution  $E_h \frac{d\sigma}{d^3 h}$  in the process  $e^+ e^- \rightarrow h \tilde{\chi}_1^+ \tilde{\chi}_1^-$ . After squaring and summing/averaging over the external spins the square of the matrix element  $\mathcal{M} = \sum_{i=1}^7 \mathcal{M}_i$  obtained from Eq. (4) with the help of FORM [18], we performed two analytic integrations of  $|\overline{\mathcal{M}}|^2$  over the phase-space variables, in the following way.

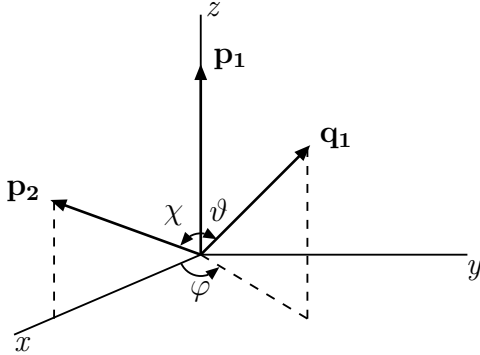


Figure 9: Angular-variables definition in the chargino-pair c.m. frame.

Starting from the momenta definition

$$e^+(p_1) + e^-(p_2) \rightarrow \tilde{\chi}_1^+(q_1) + \tilde{\chi}_1^-(q_2) + h^0(h), \quad (18)$$

and

$$p_1 = (E_1, \mathbf{p}_1), \quad p_2 = (E_2, \mathbf{p}_2), \quad q_1 = (E'_1, \mathbf{q}_1), \quad q_2 = (E'_2, \mathbf{q}_2), \quad h = (E_h, \mathbf{h}), \quad (19)$$

the Higgs momentum distribution can be expressed as

$$E_h \frac{d\sigma}{d^3\mathbf{h}} = \frac{1}{(2\pi)^5} \int \frac{|\overline{\mathcal{M}}|^2}{16s} \delta^4(p_1 + p_2 - q_1 - q_2 - h) \frac{d^3\mathbf{q}_1}{E'_1} \frac{d^3\mathbf{q}_2}{E'_2}, \quad (20)$$

where  $s = (p_1 + p_2)^2 = 2(p_1 p_2)$ .

In order to perform analytically the two non trivial integrations in Eq. (20), we first expressed  $|\overline{\mathcal{M}}|^2$  as a function of the following five independent products of momenta

$$s, (p_1 h), (p_2 h), (p_1 q_1), (p_2 q_1). \quad (21)$$

Then, we expressed  $(p_1 q_1)$  and  $(p_2 q_1)$  in the chargino-pair c.m. system (where  $\mathbf{q}_1 + \mathbf{q}_2 = \mathbf{0}$ ) as a function of the angular variables defined in Fig. 9, as follows

$$(p_1 q_1) = \frac{s_1}{4}(1 - \beta \cos \vartheta), \quad (22)$$

$$(p_2 q_1) = \frac{s_2}{4}(1 - \beta \cos \vartheta \cos \chi - \beta \sin \vartheta \sin \chi \cos \varphi). \quad (23)$$

where

$$\beta = \sqrt{1 - \frac{4M_1^2}{s + m_h^2 - 2(p_1 h) - 2(p_2 h)}}, \quad (24)$$

$$\cos \chi = 1 - \frac{2s(s + m_h^2 - 2(p_1 h) - 2(p_2 h))}{(s - 2(p_1 h))(s - 2(p_2 h))}, \quad (25)$$

and

$$s_{1,2} = s - 2(p_{1,2} h). \quad (26)$$

Then, one can write the differential cross section as

$$E_h \frac{d\sigma}{d^3\mathbf{h}} = \frac{\beta}{s(4\pi)^5} \int_{-1}^1 d\cos \vartheta \int_0^{2\pi} d\varphi |\overline{\mathcal{M}}|^2, \quad (27)$$

and perform analytically the two angular integrations. The result (that is a quite lengthy expression) is a relativistic invariant function of  $(p_1 h)$ ,  $(p_2 h)$  and  $s$ , that we call  $f(p_1, p_2, h)$  in Eq. (5).

The total cross section has been finally worked out by integrating numerically the result of Eq. (27) over the Higgs-boson momentum in the  $e^+e^-$  c.m. system (where  $\mathbf{p}_1 + \mathbf{p}_2 = 0$ ),

$$\sigma = 2\pi \int_{E_h^{\min}}^{E_h^{\max}} dE_h |\mathbf{h}| \int_{-1}^1 d\cos \theta \left[ E_h \frac{d\sigma}{d^3\mathbf{h}}((p_1 h), (p_2 h)) \right]. \quad (28)$$

In Eq.(28),

$$(p_1 h) = \frac{\sqrt{s}}{2}(E_h - |\mathbf{h}| \cos \theta), \quad (p_2 h) = \frac{\sqrt{s}}{2}(E_h + |\mathbf{h}| \cos \theta), \quad (29)$$

with  $|\mathbf{h}| = \sqrt{E_h^2 - m_h^2}$ ,  $E_h^{\min} = m_h$ , and  $E_h^{\max} = (s + m_h^2 - 4M_1^2)/(2\sqrt{s})$ .

## References

- [1] E. Accomando *et al.* [ECFA/DESY LC Physics Working Group Collaboration], *Phys. Rept.* **299** (1998) 1. [arXiv:hep-ph/9705442];  
J. A. Aguilar-Saavedra *et al.* [ECFA/DESY LC Physics Working Group Collaboration], arXiv:hep-ph/0106315;  
K. Abe *et al.* [ACFA Linear Collider Working Group Collaboration], arXiv:hep-ph/0109166;  
T. Abe *et al.* [American Linear Collider Working Group Collaboration], in *Proc. of the APS/DPF/DPB Summer Study on the Future of Particle Physics (Snowmass 2001)* ed. N. Graf, arXiv:hep-ex/0106055 ; arXiv:hep-ex/0106056 ; arXiv:hep-ex/0106057 ; arXiv:hep-ex/0106058.
- [2] J. F. Gunion, H. E. Haber, G. L. Kane and S. Dawson, *The Higgs Hunter's Guide*, Addison-Wesley, 1990.
- [3] H. P. Nilles, *Phys. Rept.* **110** (1984) 1 .
- [4] H. E. Haber and G. L. Kane, *Phys. Rept.* **117** (1985) 75 .
- [5] R. Barbieri, *Riv. Nuovo Cim.* **11** (1988) 1.
- [6] K. J. Gaemers and G. J. Gounaris, *Phys. Lett. B* **77** (1978) 379;  
A. Djouadi, J. Kalinowski and P. M. Zerwas, *Mod. Phys. Lett. A* **7** (1992) 1765 and *Z. Phys. C* **54** (1992) 255;  
J. F. Gunion, B. Grzadkowski and X. G. He, *Phys. Rev. Lett.* **77** (1996) 5172, [arXiv:hep-ph/9605326] ;  
H. Baer, S. Dawson and L. Reina, *Phys. Rev. D* **61** (2000) 013002, [arXiv:hep-ph/9906419] ;  
A. Juste and G. Merino, arXiv:hep-ph/9910301 ;  
S. Moretti, *Phys. Lett. B* **452** (1999) 338, [arXiv:hep-ph/9902214] ;  
A. Denner, S. Dittmaier, M. Roth and M. M. Weber, arXiv:hep-ph/0309274 and references therein.
- [7] G. Belanger, F. Boudjema, T. Kon and V. Lafage, *Eur. Phys. J. C* **9** (1999) 511, [arXiv:hep-ph/9811334] ;  
A. Djouadi, J. L. Kneur and G. Moultaka, *Nucl. Phys. B* **569** (2000) 53, [arXiv:hep-ph/9903218].
- [8] A. Djouadi, J. L. Kneur and G. Moultaka, *Phys. Rev. Lett.* **80** (1998) 1830, [arXiv:hep-ph/9711244]. A. Dedes and S. Moretti, *Phys. Rev. D* **60**

(1999) 015007 [arXiv:hep-ph/9812328] and Eur. Phys. J. C **10** (1999) 515. [arXiv:hep-ph/9904491] ;

G. Belanger, F. Boudjema and K. Sridhar, Nucl. Phys. B **568** (2000) 3, [arXiv:hep-ph/9904348].

[9] A. Djouadi, J. Kalinowski, P. Ohmann and P. M. Zerwas, Z. Phys. C **74** (1997) 93 [arXiv:hep-ph/9605339];  
 A. Bartl, H. Eberl, K. Hidaka, T. Kon, W. Majerotto and Y. Yamada, Phys. Lett. B **389** (1996) 538 [arXiv:hep-ph/9607388].

[10] H. Fraas, F. Franke, G. Moortgat-Pick, F. von der Pahlen and A. Wagner, arXiv:hep-ph/0303044.

[11] A. Brignole, G. Degrassi, P. Slavich and F. Zwirner, Nucl. Phys. B **631** (2002) 195 [arXiv:hep-ph/0112177] and Nucl. Phys. B **643** (2002) 79 [arXiv:hep-ph/0206101].

[12] LEPSUSYWG, ALEPH, DELPHI, L3 and OPAL experiments, note LEPSUSYWG/01-03.1 and note LEPSUSYWG/02-04.1 (<http://lepsusy.web.cern.ch/lepsusy/Welcome.html>).

[13] M. Baillargeon, F. Boudjema, F. Cuypers, E. Gabrielli and B. Mele, Nucl. Phys. B **424** (1994) 343 [arXiv:hep-ph/9307225].

[14] B. C. Allanach *et al.* [Beyond the Standard Model Working Group Collaboration], “Les Houches ‘Physics at TeV Colliders 2003’ Beyond the Standard Model Working Group: Summary report”, arXiv:hep-ph/0402295.

[15] ALEPH, DELPHI, L3, OPAL Collaborations and the LEP Higgs Working Group, LHWG Note 2001-4 [*ALEPH 2001-057, DELPHI 2001-114, L3 Note 2007, OPAL Technical Note TN699*], CERN preprint 2001;  
 OPAL Collaboration, OPAL PN524, CERN preprint 2003.

[16] R. Barate *et al.* [ALEPH, DELPHI, L3, OPAL Collaborations and LEP Working Group for Higgs boson searches], Phys. Lett. B **565** (2003) 61 [arXiv:hep-ex/0306033].

[17] S. Heinemeyer, W. Hollik and G. Weiglein, “FeynHiggsFast: A program for a fast calculation of masses and mixing angles in the Higgs sector of the MSSM”, arXiv:hep-ph/0002213.

- [18] J.A.M. Vermaseren, *Symbolic Manipulation with FORM*, published by CAN (Computer Algebra Nederland), Kruislaan 413, 1098 SJ Amsterdam, 1991, ISBN 90-74116-01-9.
- [19] A. Pukhov *et al.*, “CompHEP: A package for evaluation of Feynman diagrams and integration over multi-particle phase space. User’s manual for version 33”, arXiv:hep-ph/9908288;  
A. Semenov, “CompHEP/SUSY package”, Nucl. Instrum. Meth. A **502** (2003) 558 [arXiv:hep-ph/0205020].